Characteristics of C_3 radicals in high-density C_4F_8 plasmas studied by laser-induced fluorescence spectroscopy

K. Takizawa,[a] K. Sasaki, and K. Kadota
Department of Electronics, Nagoya University, Nagoya 464-8603, Japan

(Received 23 May 2000; accepted for publication 5 September 2000)

Spatial and temporal variations of C_3 density in high-density octafluorocyclobutane (c-C_4F_8) plasmas were examined using laser-induced fluorescence spectroscopy. The C_3 density varied slowly for a long time after the initiation of discharge, suggesting the importance of surface chemistry for the formation of C_3. Hollow-shaped spatial distributions (the C_3 density adjacent to the chamber wall was higher than that in the plasma column) were observed in the C_3 density. This result indicates that C_3 radicals are produced from fluorocarbon film on the chamber wall and are lost in the plasma column due to electron impact processes. The surface production of C_3 was also observed in the afterglow for 1 ms after the termination of rf power. The decay time constant of the C_3 density in the late (>1 ms) afterglow, where the surface production of C_3 stopped, was almost independent of discharge parameters, suggesting that the loss of C_3 due to gas-phase reactions is negligible. © *2000 American Institute of Physics.* [S0021-8979(00)06823-7]

I. INTRODUCTION

Plasma processing using fluorocarbon (CF_4, C_4F_8, etc.) plasmas is a key technology in the fabrication of semiconductor devices. A problematic process using fluorocarbon plasmas is selective dry etching of a SiO_2 layer over underlying Si and Si_3N_4 to provide contact and via holes with high aspect ratios. Fluorocarbon plasmas also attract much attention as a source of plasma-enhanced chemical vapor deposition (PECVD) of fluorinated amorphous carbon film (fluorocarbon film), which is a candidate as an insulation layer, having a low dielectric constant in next-generation ultralarge-scale integrated (ULSI) circuits. In these applications, neutral radicals in plasmas play essential roles in achieving the desired material processing. In order to optimize the performance of processing, basic understanding of fundamental processes in fluorocarbon plasmas is of great importance.

Much effort has been concentrated on investigation of CF_x radicals in fluorocarbon plasmas. The purpose of the investigation is to understand reaction kinetics of CF_x radicals in plasmas, and to identify the etchant of SiO_2 and the precursor for deposition of fluorocarbon film. For the diagnostics of CF_x radicals, several advanced methods are available, such as infrared laser absorption spectroscopy,[1] appearance mass spectrometry,[2] and laser-induced fluorescence (LIF) spectroscopy.[3,4] However, investigation of CF_x radicals is not sufficient to understand the overall reaction kinetics in fluorocarbon plasmas. A number of radicals other than CF_x probably participate in gas-phase and surface reactions. Recently, several researchers focused attention on radicals other than CF_x.[5–8] We have examined the formation process of C_2 radicals in C_4F_8 plasmas by LIF spectroscopy.[9] It has been shown in this work that C_2 radicals are mostly produced from fluorocarbon film deposited on the chamber wall.

We have recently noticed that optical emission spectra observed in C_4F_8 plasmas contain emissions from C_3 radicals. In the present work, we carried out measurements of C_3 radical density in high-density C_4F_8 plasmas by LIF spectroscopy. We examined laser-induced excitation and fluorescence spectra carefully in order to confirm that C_3 radicals were detected by LIF spectroscopy. After the assignment of spectra observed experimentally, we measured the C_3 radical density. Production and loss processes of C_3 radicals were discussed based on the characteristics of the C_3 density. To our knowledge, the present article is the first report on C_3 radicals observed in fluorocarbon plasmas.

II. EXPERIMENT

The configuration of the plasma source and the geometry of LIF spectroscopy have been described in a previous paper.[9] The plasma source was a linear machine with a uniform magnetic field of 1 kG along the cylindrical axis of the vacuum chamber. The vacuum chamber was composed of rectangular observation chambers (20 cm×20 cm×10 cm) made of stainless steel and a Pyrex glass tube 9 cm in diameter and 33 cm in length. A quartz glass discharge tube 3 cm in diameter and 25 cm in length was attached to an observation chamber. Various rf powers at 13.56 MHz were applied to an $m=1$ helical antenna wound around the discharge tube, so that high-density plasmas with a slender column diameter of 3 cm were produced by helicon-wave discharges. The plasma column was confined radially by the external magnetic field. The operating gas was pure C_4F_8 [octafluorocyclobutane ($c-C_4F_8$)]. The gas pressure was varied from 2 to 20 mTorr by changing the pumping speed at a fixed flow rate of 1.6 ccm. Since the range of the pumping speed corresponds to residence time of 2–20 s, the pumping loss of radicals is negligible in their loss processes. Plasmas were

[a]Electronic mail: k-takiza@echo.nuee.nagoya-u.ac.jp

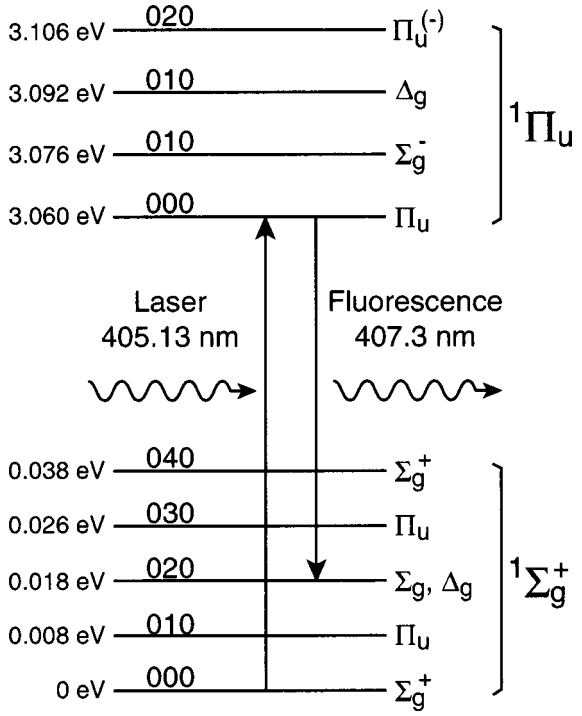

FIG. 1. Partial energy level diagram of C_3.

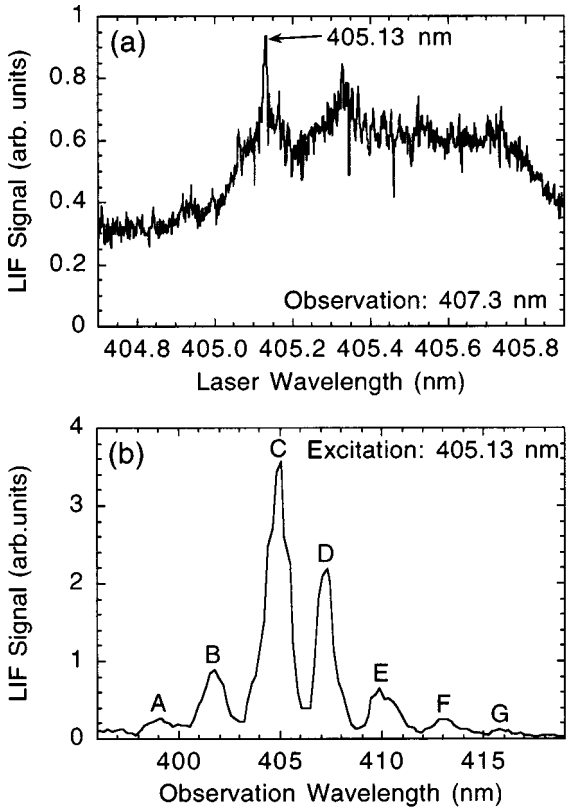

FIG. 2. Excitation (a) and observation (b) spectra in the LIF measurement. The excitation spectrum shown in (a) was obtained at an observation wavelength of 407.3 nm. The observation spectrum shown in (b) was obtained at an excitation wavelength of 405.13 nm.

produced in a pulsed mode with a repetition rate of 5 Hz and a discharge duration of 20 ms. Although the temperature of the chamber wall was not controlled throughout this study, it was not far from room temperature because of the low duty factor of the pulsed discharge.

A tunable dye laser pumped by an excimer laser was used for the LIF measurement. The dye laser beam was launched into the observation chamber through a horizontal port. A beam dump was installed at the horizontal port of the opposite side to eliminate stray light. The distance between the laser beam and the end of the helical antenna was approximately 10 cm. The LIF emission was detected through an upper port using a monochromator and a photomultiplier tube. The spatial (radial) distribution of the C_3 density along the path of the dye laser beam was obtained by changing the observation position of the LIF emission. Although the wall of the observation chamber was located ± 10 cm from the center of the plasma column, the size of the upper observation port restricted the measurements to a region of $-7 \leqslant r \leqslant 7$ cm.

III. SCHEME OF LIF

Energy levels of C_3 have been investigated by Gausset *et al.* in detail.[10] A partial energy level diagram of C_3 is shown in Fig. 1. The ground and first excited states of C_3 are $\tilde{X}^1\Sigma_g^+$ and $\tilde{A}^1\Pi_u$, respectively, and the present LIF measurements were carried out on the $\tilde{A}^1\Pi_u - \tilde{X}^1\Sigma_g^+$ transition. Since the energy separations among vibrational states are of the order of room temperature, vibrational states up to 040 of $\tilde{X}^1\Sigma_g^+$ have considerable population. In the present work, the wavelengths employed for excitation and observation in the LIF measurement were determined experimentally through detailed spectral analyses. Figure 2(a) shows an example of an excitation spectrum, which was obtained by tuning the wavelength of the dye laser at a fixed observation wavelength of 407.3 nm [emission D in Fig. 2(b)]. This spectrum corresponds partly to the 000–000 $\Pi_u - \Sigma_g^+$ band excitation. Because of the strong fluorescence emission, we chose an excitation wavelength at 405.13 nm.

Figure 2(b) shows an observation spectrum at a fixed excitation wavelength of 405.13 nm. The wavelength resolution in the measurement was 0.3 nm. Fluorescence emissions at seven wavelengths, which are denoted by indexes A–G, were observed in the wavelength range of 396–419 nm. Although the wavelength of emission C overlapped that of the dye laser, stray light was negligible in this measurement. By considering the low potential energies of vibrational states of $\tilde{X}^1\Sigma_g^+$ and the linewidth of the dye laser pulse ($\sim 0.2\,\mathrm{cm}^{-1}$), fluorescence emissions A–G can be assigned as shown in Table I. The fluorescence spectrum can be explained reasonably by taking into account simultaneous excitations on 000–000 $\Pi_u - \Sigma_g^+$, 010–010 $\Sigma_g^- - \Pi_u$, 010–030 $\Delta_g - \Pi_u$, and 020–040 $\Pi_u^{(-)} - \Sigma_g^+$ bands at a wavelength of 405.13 nm. According to Table I, C_3 radicals at the ground state can be detected with high sensitivity when we choose the observation wavelength of 407.3 nm (emission D). Based on the spectral analyses described above, we employed excitation and observation wavelengths at 405.13 and 407.3 nm, respectively, so that we measured the density of C_3 radicals at the ground state by LIF spectroscopy.

TABLE I. Assignment of energy levels for fluorescence emissions shown in Fig. 2(b).

	Excitation	Fluorescence		
Index	$\tilde{X}^1\Sigma_g^+$	$\tilde{A}^1\Pi_u$	$\tilde{X}^1\Sigma_g^+$	
A	$040\Sigma_g^+$	$020\ \Pi_u^{(-)}$	$000\Sigma_g^+$	
B	$030\Pi_u$	$010\ \Delta_g$	$010\ \Pi_u$	Overlapping
	$040\ \Sigma_g^+$	$020\ \Pi_u^{(-)}$	$020\ \Sigma_g, \Delta_g$	
	$000\ \Sigma_g^+$	$000\ \Pi_u$	$000\ \Sigma_g^+$	
C	$010\ \Pi_u$	$010\ \Sigma_g^-$	$030\ \Pi_u$	Overlapping
	$030\Pi_u$	$010\ \Delta_g$	$030\ \Pi_u$	
	$040\Sigma_g^+$	$020\ \Pi_u^{(-)}$	$040\ \Sigma_g^+$	
D	$000\Sigma_g^+$	$000\ \Pi_u$	$020\ \Sigma_g, \Delta_g$	
E	$000\Sigma_g^+$	$000\ \Pi_u$	$040\ \Sigma_g^+$	
F	$000\Sigma_g^+$	$000\ \Pi_u$	(060)	Speculation
G	$000\Sigma_g^+$	$000\ \Pi_u$	(080)	Speculation

IV. RESULTS AND DISCUSSION

A. Long-term temporal variation

First of all, we measured long-term variation of the C_3 density after the ignition of a C_4F_8 plasma. Before starting the experiment, the chamber wall was cleaned sufficiently (fluorocarbon film on the chamber wall was removed) using a continuous wave (cw) oxygen discharge. After the chamber wall was initialized by the oxygen discharge, a C_4F_8 plasma was produced at a rf power of 1 kW and a gas pressure of 2 mTorr. The C_3 density was measured 20 μs after the termination of the rf power in each pulsed discharge to eliminate electrical noise. Since 20 μs is much shorter than diffusion and reaction time constants, we can obtain the C_3 density in the discharge phase by this method. Figure 3(a) shows the temporal variation of the C_3 density at an observation position 6 cm away from the center of the plasma column. At the beginning of the discharge (0–2 min), no C_3 radicals were detected. After 2 min, the C_3 density increased gradually, and was saturated at $t \simeq 15$ min.

In Fig. 3(b), a CF_4 plasma at a rf power of 1 kW and a gas pressure of 2 mTorr was produced after oxygen cleaning discharge. As is shown, no C_3 radicals were detected in the CF_4 plasma. At $t=60$ min, the gas was exchanged for C_4F_8. Six min after the exchange of the gas, a gradual increase in the C_3 density was observed. The period with no C_3 density was longer in Fig. 3(b) than in Fig. 3(a).

Another experimental procedure was carried out in Fig. 3(c). The experiment started after sufficient seasoning discharge at a rf power of 1 kW and a C_4F_8 pressure of 5 mTorr. In Fig. 3(c), the saturation level of the C_3 density is shown for 0–5 min. At $t=5$ min, the gas was exchanged for Ar at a pressure of 5 mTorr. As is shown, the C_3 density in the Ar plasma was negligible even though the chamber wall was covered with fluorocarbon film formed by the C_4F_8 seasoning discharge. When the gas was exchanged for C_4F_8 again at $t=15$ min, the C_3 density recovered the saturation level immediately. At $t=25$ min, the gas was exchanged for CF_4 at a pressure of 5 mTorr. In the CF_4 plasma, the C_3 density was approximately 2/3 that in the C_4F_8 plasma. A gradual decrease in the C_3 density was observed in the CF_4 plasma. When the C_4F_8 plasma was restored at $t=60$ min, the C_3 density recovered the saturation level immediately.

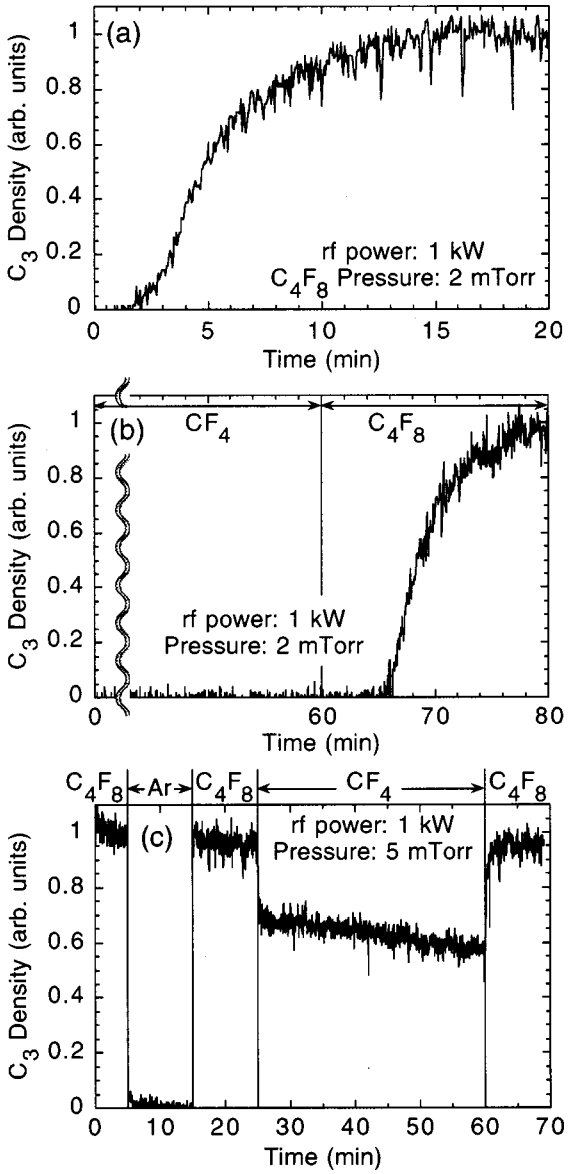

FIG. 3. Long-term temporal variations of the C_3 density at an observation position 6 cm from the center of the plasma column. The rf power was 1 kW. The gas pressure was 2 mTorr in (a) and (b) and 5 mTorr in (c). (a) Gradual increase in the C_3 density after the ignition of a C_4F_8 plasma. The chamber wall was cleaned initially by an oxygen discharge. (b) C_3 densities measured in CF_4 and C_4F_8 plasmas. The chamber wall was cleaned initially by an oxygen discharge. (c) C_3 densities measured in Ar and CF_4 plasmas after seasoning discharge using a C_4F_8 plasma.

B. Spatial distribution and surface production

Figure 4 shows radial distributions of the C_3 density along the path of the dye laser beam. The rf power was varied at a fixed gas pressure of 2 mTorr in Fig. 4(a), while in Fig. 4(b) the gas pressure was varied at a fixed rf power of 1 kW. The measurements were carried out after the long-term variation in the C_3 density was saturated. The position $r=0$ cm corresponds to the center of the plasma column, and the walls of the rectangular observation chamber were lo-

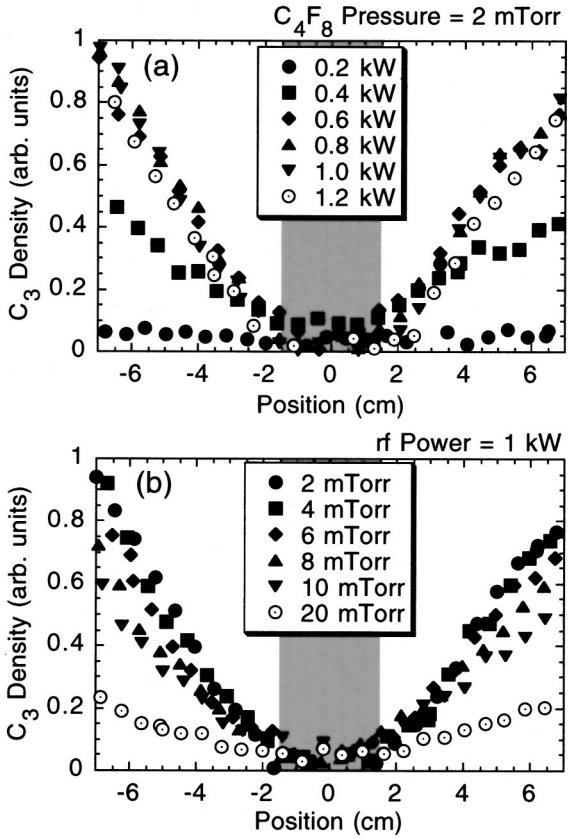

FIG. 4. Radial distribution of the C_3 density along the path of the dye laser beam. The rf power was varied at a fixed gas pressure of 2 mTorr in (a), while in (b) the gas pressure was varied at a fixed rf power of 1 kW.

cated at $r=\pm 10$ cm. The high-density plasma column was localized in the hatched region ($-1.5 \leqslant r \leqslant 1.5$ cm) by the external magnetic field. As shown in Fig. 4, radial distributions of the C_3 density were hollow for all discharge conditions. The C_3 density in the plasma column was much lower than that in the outside region.

Hollow-shaped radial distributions have been observed in CF, CF_2, and C_2 densities in C_4F_8 plasmas produced in the same machine.[9,11–13] As has been discussed in previous papers, the following reaction and transport mechanisms are understood from the hollow-shaped density distribution. The hollow-shaped density distribution is maintained stationarily by loss processes (sink) in the plasma column and production processes (source) in the outside region. C_3 radicals produced in the outside region are transported toward the plasma column due to diffusion. Electron impact dissociation and ionization play the role of sink in the plasma column, while the source of C_3 in the outside region is, reasonably, considered to be the surface of the chamber wall. Production of C_3 due to electron impact dissociation of C_4F_8 is probably not expected. In no papers concerned with disassociation processes of C_4F_8, is the production of C_3 by electron impact considered.[14–16] In addition, production of C_3 due to association among C and C_2 may not also be expected in the low gas pressure below 20 mTorr. Accordingly, gas-phase production of C_3 may be negligible. In the spatial distributions shown in Fig. 4, the C_3 densities in the plasma column are close to zero, which is consistent with the assumption

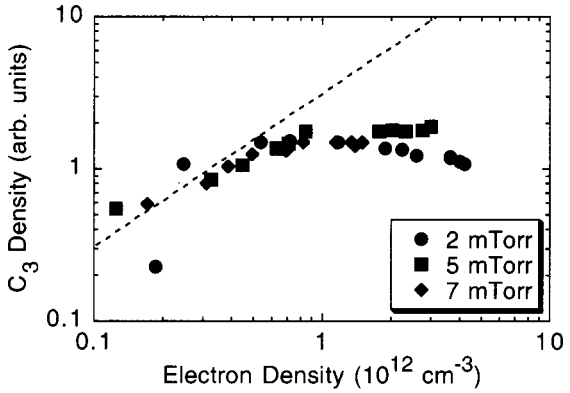

FIG. 5. Relationship between the C_3 density at $r=-6$ cm and the electron density in the plasma column.

that the production of C_3 in the gas phase is negligible. The hollow-shaped density distribution provides direct evidence that C_3 radicals are produced from the surface of the chamber wall covered with fluorocarbon film.

The surface production of C_3 is consistent with the long-term variation in the C_3 density shown in Fig. 3(a). At the beginning of discharge, there is no fluorocarbon film on the chamber wall, resulting in the negligible C_3 density. The time constant of the gradual increase in the C_3 density may be closely related with the growth of fluorocarbon film on the chamber wall. The property of fluorocarbon film may be significantly different between CF_4 and C_4F_8 plasmas, resulting in the negligible C_3 density in CF_4 plasmas shown in Fig. 3(b). Contrary to the result shown in Fig. 3(b), a considerable amount of C_3 was detected in the CF_4 plasma after the seasoning discharge using C_4F_8, indicating the importance of fluorocarbon film formed by the C_4F_8 plasma. The gradual decrease in the C_3 density observed in the CF_4 plasma shown in Fig. 3(c) may be due to a change in the property of the fluorocarbon film. The mechanism of surface production of C_3 is not physical sputtering of fluorocarbon film, since no C_3 radicals were detected in the Ar discharge even though the chamber wall was covered with thick fluorocarbon film formed by the C_4F_8 seasoning discharge. It is necessary to supply fluorocarbon neutral radicals and/or ions for surface production of C_3. The rapid decrease in the C_3 density just after the change of operating gas from C_4F_8 to CF_4 indicates the importance of the chemical composition of the particle flow supplied by the gas phase (it is expected that the property of fluorocarbon film does not change right after the change of the operating gas).

In the present plasma source, a higher electron density was obtained for a higher rf power and a lower gas pressure.[17] The higher electron density for a lower gas pressure may be attributed to the fact that the excitation efficiency of a helicon wave decreases with increasing gas pressure.[18] Considering the above characteristics of the electron density, it is known from Fig. 4 that the aspect ratio of the hollow-shaped distribution becomes higher for a higher electron density. In Fig. 5, we have plotted the C_3 density at $r=-6$ cm as a function of the electron density in the plasma column. The electron density was measured using a micro-

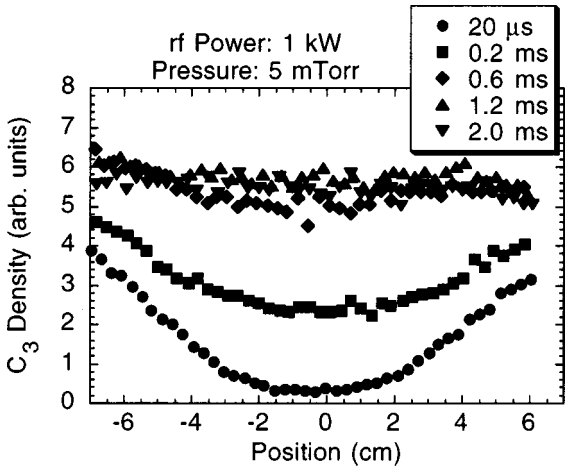

FIG. 6. Radial distribution of the C_3 density at various times after the termination of the rf power.

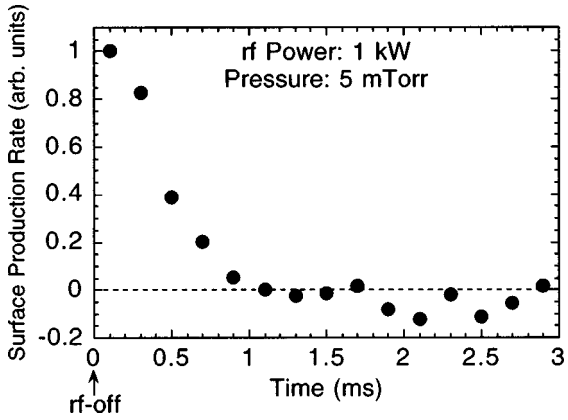

FIG. 7. Temporal variation in the surface production rate of C_3 in the afterglow.

wave interferometer. In order to separate the influence of the property of fluorocarbon film from the effect of electron density, the chamber wall was seasoned sufficiently by a C_4F_8 discharge at a rf power of 1 kW and a pressure of 10 mTorr. The C_3 density at each discharge condition was measured after supplying the sufficient seasoning discharge. This seasoning procedure made the surface condition identical before measurements at each discharge condition. The measurements at each discharge condition were carried out rapidly to avoid changes in surface conditions. As shown in Fig. 5, a unique relationship was roughly found between the C_3 and electron densities, even though the discharge condition was varied in wide ranges of 0.1–1.5 kW and 2–7 mTorr. This result suggests the contribution of ion bombardment to the surface production of C_3. Other possible mechanisms to explain the result shown in Fig. 5 are the change in the chemical composition of gas-phase radicals and the increase in the intensity of vacuum ultraviolet (VUV) emission with the electron density. As has been reported previously, a unique relationship has also been found between the C_2 and electron densities.[9] However, the relation between the C_3 and electron densities for $n_e < 10^{12}\,\mathrm{cm}^{-3}$ ($n_{C_3} \propto n_e$ is evaluated from Fig. 5) is more gradual than that between C_2 and electron densities ($n_{C_2} \propto n_e^{1.4}$). Hence the surface production of C_3 is less sensitive to the degree of ion bombardment in comparison with the surface production of C_2.

C. Temporal variation in the afterglow

Figure 6 shows photographs of radial distributions of the C_3 density at various times after the termination of the rf power. The rf power in the discharge phase was 1 kW and the C_4F_8 gas pressure was 5 mTorr. The distribution at $t = 20$ μs represents the profile in the discharge phase since the time constants for diffusion and reactions are much longer than 20 μs. As shown in Fig. 6, the hollow-shaped distribution in the discharge phase changed into a uniform one in the afterglow. This is because the electron temperature in the plasma column rapidly decreases below 1 eV in the afterglow,[19,20] resulting in the disappearance of electron impact dissociation and ionization of C_3 at the center. The center region of the hollow-shaped distribution is filled by diffusion of C_3 from the outside region. In addition to the change in the spatial profile, it is seen from Fig. 6 that the C_3 density increases in the afterglow. A similar increase in the afterglow has been observed in the CF_2 density.[21] After the increase in the C_3 density stopped, the C_3 density decreased slowly while keeping a uniform distribution.

The increase in the C_3 density indicates production of C_3 in the afterglow. This may be a part of surface production that is observed in the discharge phase. In the discharge phase, the steady-state C_3 density is maintained by the balance between loss and production of C_3. In the afterglow, loss of C_3 due to electron impact dissociation and ionization disappears, while the surface production of C_3 continues, resulting in the increase in the C_3 density. Figure 5 suggests that there is a surface production process which is dependent on the degree of ion bombardment. In the afterglow, the degree of ion bombardment becomes much weaker than that in the discharge phase since the plasma potential drops rapidly after termination of the rf power. Therefore, the increase in the C_3 density in the afterglow indicates that there is another surface production process which does not require ion bombardment.

Temporal variation in the surface production rate in the afterglow was evaluated from the temporal variation in the spatial distribution of the C_3 density shown in Fig. 6. The surface production rate was derived from the increase in the C_3 density by $\Delta N_{C_3}(t)/(\Delta TS)$, where $\Delta N_{C_3}(t)$ is the variation in the number of C_3 radicals contained in the chamber defined by $\Delta N_{C_3}(t) = \int_V n_{C_3}(t + \Delta T/2)\mathrm{d}V - \int_V n_{C_3}(t - \Delta T/2)\mathrm{d}V$, ΔT is the time step in the evaluation, and S is the surface area of the chamber wall. As shown in Fig. 7, the surface production rate decreased monotonically and was negligible in the late afterglow of $t \geqslant 1$ ms. Since the duration of the surface production is comparable to the decay time constant of the C_2 density,[9] there is a possibility that C_2 radicals contribute to the surface production of C_3. However, the mechanism of the surface production of C_3 has not been fully understood yet.

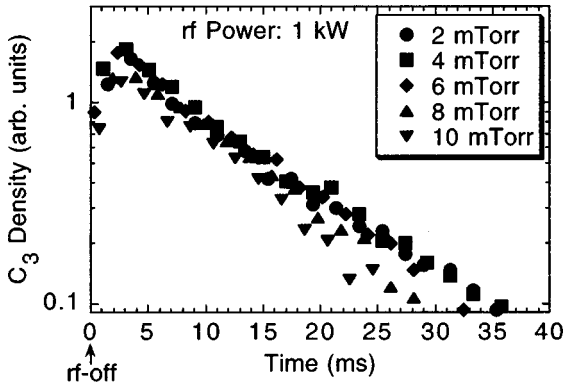

FIG. 8. Temporal variation in the C_3 density at $r=-6$ cm in the afterglow.

Figure 8 shows the temporal variation of the C_3 density at $r=-6$ cm in the afterglow for various gas pressures. The rf power in the discharge phase was fixed at 1 kW. The increase in the initial afterglow corresponds to the surface production of C_3 mentioned above. As shown in Fig. 8, the temporal decrease in the late afterglow was approximated well with exponential functions. The decay time constant of the C_3 density was almost independent of the gas pressure, and was approximately 9–13 ms. The constant lifetime suggests that loss of C_3 due to gas-phase reactions is negligible. The dominant loss process of C_3 in the afterglow is probably diffusion and surface loss on the chamber wall. The lifetime of 9–13 ms is much longer than that of C and C_2 observed in the same machine.[9] The surface loss probability corresponding to the lifetime of 9–13 ms is approximately 0.02.[22] The long lifetime and the small surface loss probability are consistent with overall knowledge that C_3 is a relatively stable molecule in the C_n family.[23]

V. CONCLUSIONS

We have carried out diagnostics of C_3 radicals in high-density C_4F_8 plasmas by laser-induced fluorescence spectroscopy. The C_3 densities had hollow-shaped radial distributions, indicating the surface production of C_3 from fluorocarbon film deposited on the chamber wall. Ion bombardment to fluorocarbon film partly contributes to the surface production in the discharge phase. An increase in the C_3 density has been observed in the initial afterglow for 1 ms after the termination of the rf power, indicating the existence of a surface production process that does not require ion bombardment. The decay time constant of the C_3 density in the late afterglow has been much longer than the lifetimes of C and C_2. To our knowledge, the present work is the first paper reporting characteristics of C_3 radicals in fluorocarbon plasmas. The mechanism of surface production of C_3 is not known; further investigation of C_3 radicals is necessary.

[1] M. Magane, N. Itabashi, N. Nishiwaki, T. Goto, C. Yamada, and E. Hirora, Jpn. J. Appl. Phys., Part 2 **29**, L829 (1990).
[2] H. Sugai and H. Toyoda, J. Vac. Sci. Technol. A **10**, 1193 (1992).
[3] J. P. Booth, G. Hancock, N. D. Perry, and M. Toogood, J. Appl. Phys. **66**, 5251 (1989).
[4] C. Suzuki, K. Sasaki, and K. Kadota, J. Appl. Phys. **82**, 5321 (1997).
[5] W. W. Stoffels, E. Stoffels, and K. Tachibana, J. Vac. Sci. Technol. A **16**, 87 (1998).
[6] W. Schwarzenbach, G. Cunge, and J. P. Booth, J. Appl. Phys. **85**, 7562 (1999).
[7] K. Teii, M. Hori, M. Ito, and T. Goto, J. Vac. Sci. Technol. A **18**, 1 (2000).
[8] K. Sasaki, K. Takizawa, N. Takada, and K. Kadota, Thin Solid Films (to be published).
[9] C. Suzuki, K. Sasaki, and K. Kadota, Jpn. J. Appl. Phys., Part 1 **38**, 6896 (1999).
[10] L. Gausset, G. Herzberg, A. Lagerqvist, and B. Rosen, Astrophys. J. **142**, 45 (1965).
[11] C. Suzuki, K. Sasaki, and K. Kadota, J. Vac. Sci. Technol. A **16**, 2222 (1998).
[12] K. Sasaki, H. Furukawa, C. Suzuki, and K. Kadota, Jpn. J. Appl. Phys., Part 2 **38**, L954 (1999).
[13] K. Sasaki, H. Furukawa, C. Suzuki, and K. Kadota, J. Appl. Phys. (to be published).
[14] H. Toyoda, M. Iio, and H. Sugai, Jpn. J. Appl. Phys., Part 1 **36**, 3730 (1997).
[15] H. Kazumi and K. Tago, Jpn. J. Appl. Phys., Part 1 **34**, 2125 (1995).
[16] H. Hayashi, S. Morishita, T. Tatsumi, Y. Hikosaka, S. Noda, H. Nakagawa, S. Kobayashi, M. Inoue, and T. Hoshino, J. Vac. Sci. Technol. A **17**, 2557 (1999).
[17] K. Sasaki, K. Ura, K. Suzuki, and K. Kadota, Jpn. J. Appl. Phys., Part 1 **36**, 1282 (1997).
[18] K. P. Schamrai and T. B. Taranov, Plasma Phys. Controlled Fusion **36**, 1719 (1994).
[19] N. Takada, D. Hayashi, K. Sasaki, and K. Kadota, Jpn. J. Appl. Phys., Part 2 **36**, L1702 (1997).
[20] D. Hayashi, M. Nakamoto, N. Takada, K. Sasaki, and K. Kadota, Jpn. J. Appl. Phys., Part 1 **38**, 6084 (1999).
[21] C. Suzuki, K. Sasaki, and K. Kadota, Jpn. J. Appl. Phys., Part 1 **37**, 5763 (1998).
[22] P. J. Chantry, J. Appl. Phys. **62**, 1141 (1987).
[23] M. E. Geusic, M. F. Jarrold, T. J. McIlrath, R. R. Freeman, and W. L. Brown, J. Chem. Phys. **86**, 3862 (1987).